

Effect of processing routes on properties of plasma melted intermetallic Ti-Al-Ta ingots

J. Lapin^{1*}, K. Frkáňová²

¹*Institute of Materials and Machine Mechanics, Slovak Academy of Sciences,
Račianska 75, 831 02 Bratislava, Slovak Republic*

²*Slovak University of Technology, Faculty of Materials Science and Technology,
Paulínska 16, 917 24 Trnava, Slovak Republic*

Received 14 April 2011, received in revised form 23 June 2011, accepted 24 June 2011

Abstract

The effect of two processing routes on chemical composition, microstructure and mechanical properties of plasma melted intermetallic ingots with nominal composition Ti-46Al-8Ta (at.%) was studied. The semi-products for plasma melting were prepared by: (i) cold single action compaction of initial pure materials and (ii) induction melting of binary master alloy with nominal composition Al-14Ta (at.%), its casting in a copper mould and mixing with Ti sponge. The applied processing routes and selected parameters of plasma melting result in a full dissolution of initial materials and homogeneous distribution of alloying elements in the plasma melted Ti-Al-Ta ingots. The ingots prepared from the cold compacted materials show high burnout of Al up to 3.7 at.% and contamination by O up to 1.31 at.%. Content of Al is well adjusted in the plasma melted ingots prepared from the master alloy mixed with Ti sponge and content of O is reduced to 0.69 at.%. The morphology of dendrites within columnar and equiaxed grains indicates solidification via β (Ti-based solid solution with cubic crystal structure) primary solidification phase. The microstructure of the grains is lamellar and consists of α_2 (Ti₃Al) and γ (TiAl) phases. Vickers hardness and compression yield strength of the plasma melted ingots is higher than those measured in a benchmark Ti-46Al-8Ta (at.%) alloy with convoluted $\gamma + \alpha_2$ type of microstructure. The compression strength of the ingot prepared from the cold compacted semi-products is by 20 % higher than that of the ingot prepared from the master Al-Ta alloy mixed with the Ti sponge.

Key words: titanium aluminides, TiAl, melting, microstructure, mechanical properties

1. Introduction

Due to low density, high specific strength, high Young's modulus and oxidation resistance at high temperatures, TiAl-based alloys represent a good alternative to nickel-based superalloys currently in use. A major effort has been made over the last twenty years to introduce these materials into the marketplace as engineering components. Nowadays, TiAl-based alloys are used as high-temperature structural materials for low pressure turbine blades of modern aircraft engines [1–3], turbocharger wheels [4, 5] and automotive exhaust valves [6, 7]. However, metallurgical processing including melting and casting of these alloys is still constrained by several limitations due to

high reactivity of the melt [8–11] and the strong influence of the alloy chemistry on microstructure and mechanical properties [12, 13]. The most important factors affecting ingot metallurgy of TiAl-based alloys are: (i) amounts of specific alloying elements including impurities and (ii) applied melting process. Several ingot manufacturing techniques are suitable for processing of TiAl-based alloys: (i) vacuum arc remelting (VAR) [14], (ii) plasma arc melting (PAM) [15], (iii) electron beam melting (EBM) [14], and (iv) induction skull melting (ISM) [16]. Among those methods, plasma melting enables to achieve extremely high temperatures of the plasma arc with turbulent gas flow, which allows good mixing of alloying elements in the liquid bath for good chemical homogeneity of processed

*Corresponding author: tel.: +421 2 49268290; fax: +421 2 49268312; e-mail address: ummslapi@savba.sk



Fig. 1. Initial pure materials used for processing of semi-products.

ingots [15]. Melting under inert gas (Ar or He) prevents high evaporation of alloying elements such as Al or Cr. Plasma melting in a cold hearth avoids alloy contamination by the crucible and allows preparing ingots of the highest purity [15].

The aim of the present work is to study the effect of two processing routes on chemical composition, microstructure and mechanical properties of plasma melted ingots with nominal composition Ti-46Al-8Ta (at.%). The studied alloy belongs to the 4th generation of cast TiAl-based alloys also called as “airhardenable”, which have been designed to form fine grain structure at low cooling rates during heat treatments [17–19].

2. Experimental procedure

2.1. Processing of semi-products for plasma melting

Semi-products for plasma melting were prepared from initial pure materials in the form of titanium sponge (purity of 99.39 % and oxygen content of 600 wtppm), pieces of aluminium with dimensions $5 \times 5 \times 2 \text{ mm}^3$ (purity of 99.998 % and oxygen content of 30 wtppm) and tantalum chips with dimensions $1 \times 2 \times 0.3 \text{ mm}^3$ (purity of 99.95 % and oxygen content of 150 wtppm), as shown in Fig. 1.

Two processing routes were applied: (i) cold single action compaction and (ii) induction melting of master alloy with nominal composition Al-14Ta (at.%), its casting in a cold copper mould and mixing with the Ti sponge. The cold single action compaction of cylindrical Ti-Al-Ta semi-products was performed at various compacting pressures ranging from 215 to 645 MPa in a metallic die with a diameter of 34 mm. The induction melting of the master alloy was car-

ried out in Al_2O_3 -based crucible (purity 95 %) with an inner diameter of 60 mm and length of 110 mm under a preliminary vacuum of 5 Pa. When aluminium started evaporating, furnace was filled up with argon (purity 99.995 %) to a pressure of 30 kPa and the melt was stabilised at a temperature of about 1600°C for various time ranging from 60 to 270 s. After the stabilisation the melt was cast into a cold copper mould with a diameter of 20 mm and length of 90 mm.

2.2. Plasma melting

Both types of the semi-products, i.e. the cold compacted Ti-Al-Ta initial materials and induction melted master Al-Ta ingots mixed with the Ti sponge, were melted in a plasma furnace with a horizontal water cooled copper hearth. To study the effect of applied processing routes on chemical composition, microstructure and mechanical properties of the plasma melted ingots, other processing parameters of the plasma melting were fixed as follows: (i) argon flow rate of 50 l min^{-1} , (ii) constant rate of relative movement of plasma torch of $v = 170 \text{ cm h}^{-1}$, (iii) four plasma torch passes and (iv) maximum temperature of the melt of about 1650°C. Dimensions of the cold hearth allowed preparing ingots with a maximum size of $30 \times 30 \times 270 \text{ mm}^3$ and a maximum weight up to 1.3 kg.

2.3. Ingot characterisation

Microstructure of the semi-products and plasma melted ingots was studied by optical microscopy (OM) and backscattered scanning electron microscopy (BSEM). OM and BSEM samples were prepared using standard metallographic techniques and etched in a reagent of 150 ml H_2O , 25 ml HNO_3 and 10 ml HF. Quantitative metallography was performed on digitalized OM micrograph using computerized image analysis and software SigmaScanPro 5.

Chemical composition was measured by energy-dispersive spectroscopy (EDX) and laser induced breakdown spectroscopy (LIBS) using a laser elemental analyzer LEA S500. Oxygen content was measured with a LECO TC-436 N/O apparatus. For the oxygen measurements, analysed samples with a diameter of 8 mm and length of 20 mm were cut from the plasma melted ingots. The surface layer was removed by grinding and the samples were carefully drilled to achieve fine chips. The melting of the chips was performed in a graphite crucible under helium. Oxygen was detected in the form of carbon dioxide using infrared detection.

Vickers hardness measurements were performed at an applied load of 298 N. Average Vickers hardness values were calculated from 30 independent measurements. Cylindrical compression specimens with a dia-

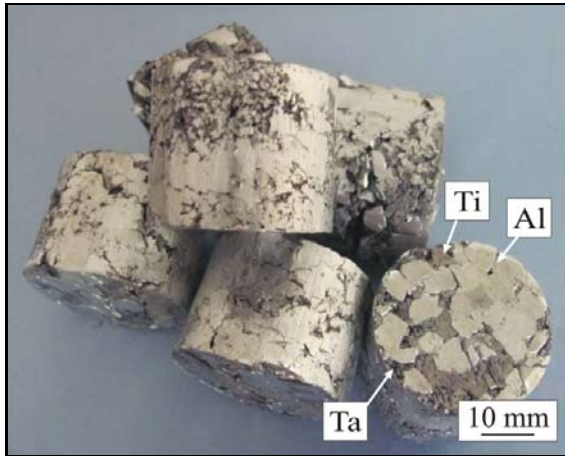


Fig. 2. Cylindrical Ti-Al-Ta semi-products prepared by cold single action compaction.

meter of 6 mm and length of 9 mm were lathe machined from the plasma melted ingots. The surface of the compression specimens was polished to a roughness better than $0.3 \mu\text{m}$. Room temperature compression tests were performed on a universal testing machine Zwick at an initial strain rate of $1 \times 10^{-4} \text{s}^{-1}$. Compression force needed for disintegration of the cold compacted cylindrical Ti-Al-Ta semi-products was measured in a direction perpendicular to their longitudinal axis using a cylindrical punch with a diameter of 40 mm.

3. Results and discussion

3.1. Cold single action compaction

Figure 2 shows the typical examples of the cold compacted Ti-46Al-8Ta (at.%) semi-products with a diameter of 34 mm and height up to 30 mm. Densification of the semi-products D_m was calculated according to a relationship in the form

$$D_m = \frac{\rho_c}{\rho_t} 100, \quad (1)$$

where ρ_c is the measured density of the cold compacted semi-products and ρ_t is the theoretical density of the Ti-46Al-8Ta (at.%) alloy. Both the densities ρ_c and ρ_t were determined from measured dimensions and weight of cylindrical samples according to relationship

$$\rho_i = \frac{4m}{\pi d_i^2 h_i}, \quad (2)$$

where m is the weight, d is the diameter, and h is the height of the measured samples. The index i is associated with c and t in the case of the cold

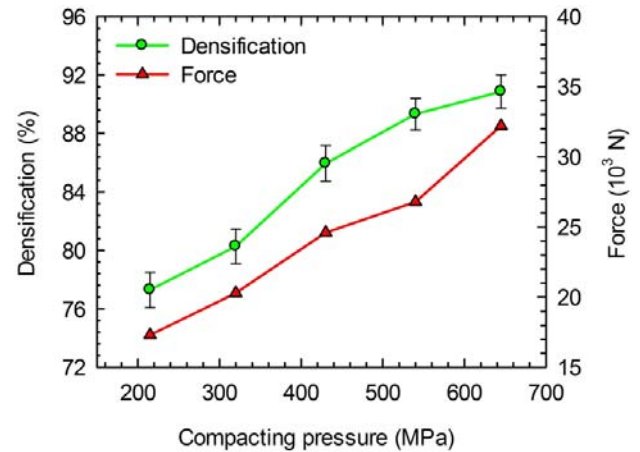


Fig. 3. Dependence of densification and force for disintegration of the cold compacted semi-products on applied compacting pressure.



Fig. 4. Cast ingot from induction melted master Al-Ta alloy.

compact semi-products and fully dense Ti-46Al-8Ta (at.%) alloy, respectively. The theoretical density of Ti-46Al-8Ta (at.%) alloy is measured to be $\rho_t = (4.960 \pm 0.009) \text{g cm}^{-3}$ using two fully dense cylindrical samples with a diameter of 12 mm and length of 140 mm, which were prepared by plasma melting, centrifugal casting and hot isostatic pressing at a temperature of 1260°C and applied pressure of 200 MPa for 4 h. Figure 3 shows dependence of densification and force needed for disintegration of the semi-products on applied compacting pressure. Both the densification and force for disintegration increase with increasing compacting pressure. An optimal compacting pressure is determined to be between 430 and 530 MPa. The applied pressures lower than 430 MPa lead to an insufficient strength of the semi-products and relieve of the Ta chips during handling. The applied pressures higher than 530 MPa lead to a difficult relieve of the semi-products from the metallic die and high wear of the die.

3.2. Induction melting of master alloy

Figure 4 shows the typical example of the induc-

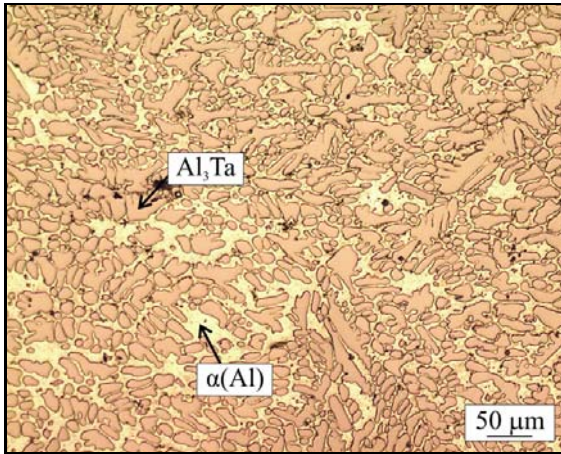


Fig. 5. OM micrograph showing dendritic microstructure of master Al-Ta alloy.

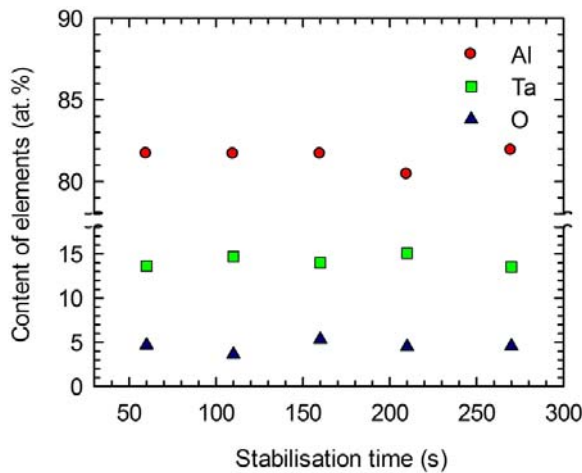


Fig. 6. Dependence of content of Al, Ta and O on stabilisation time of the melt during induction melting of master Al-Ta alloy.

tion melted master Al-14Ta (at.%) alloy with a weight of 0.44 kg, which was cast into the cold copper mould. According to a binary phase diagram [20], liquidus temperature of the master alloy is 1527°C, which is significantly lower than that of 2997°C of pure tantalum. Figure 5 shows dendritic microstructure of the cast master ingots. The dendrites are composed of 71.4 at.% Al and 28.6 at.% Ta that according to the binary phase diagram [20] represents Al₃Ta intermetallic phase. Interdendritic region consists of 98.1 at.% Al in the form of α(Al) solid solution. Figure 6 shows variation of average content of Al, Ta and O with stabilisation time of the melt on a temperature of about 1600°C. The average content of Al, Ta and O is measured to be (81.5 ± 1.1) at.%, (14.2 ± 0.8) at.% and (4.3 ± 0.7) at.%, respectively. The contamination of the cast ingots by oxygen results from a reaction of the melted alloy with Al₂O₃-based crucible. Visual observations of the Al₂O₃-based crucible clearly showed evidence of deterioration of the crucible walls by the melt.

3.3. Plasma melting

3.3.1. Chemical composition and homogeneity of ingots

Figure 7 illustrates the typical example of plasma melted Ti-Al-Ta ingot. The surface of the ingot contains two different regions: (i) “weld bead” type of the surface where the plasma torch passed along the ingot at a constant rate of 170 cm h⁻¹ and (ii) “flat” type of the surface where the plasma torch was stopped. The width and length of the plasma melted ingots were constant of 30 and 270 mm, respectively. The height of the ingots varied between 14 and 30 mm and weight between 0.8 and 1.3 kg depending on the weight of the melted semi-products. Each plasma melted ingot was cut in a direction perpendicular to its longitudinal axis along marked positions 1, 2 and 3 (Fig. 7) to four

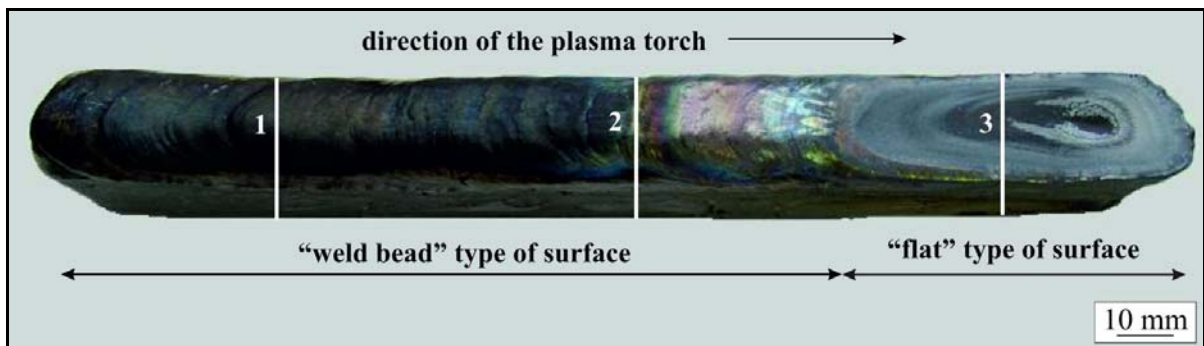


Fig. 7. Plasma melted Ti-Al-Ta ingot prepared from the master Al-Ta alloy mixed with the Ti sponge. Longitudinal positions for the measurements of chemical composition, microstructure evaluation and extraction of compression specimens are indicated by the lines 1, 2 and 3.

Table 1. Nominal and chemical compositions of benchmark alloy, semi-products and plasma melted ingots

Element	Benchmark alloy	Cold compacted semi-products		Master Al-Ta alloy with Ti sponge	
	Chemical composition (at.%)	Nominal composition (at.%)	Chemical composition of plasma melted ingots (at.%)	Nominal composition (at.%)	Chemical composition of plasma melted ingots (at.%)
Ti	base	46.0	base	45.0	base
Al	45.90	46.0	42.30	47.0	46.00
Ta	7.90	8.0	8.60	8.0	8.90
O	0.26	–	1.31	–	0.69

pieces and subjected to evaluation of chemical composition, microstructure, Vickers hardness and room temperature compression properties.

Microstructural and chemical analyses of the plasma melted ingots show that the initial materials including hardly meltable Ta chips were fully dissolved and homogeneously distributed. The local chemical composition measured in the periphery and middle parts of the ingots varied within the experimental error of the measurements. Table 1 summarises nominal composition of the semi-products and measured chemical composition of a benchmark Ti-46Al-8Ta (at.%) alloy and plasma melted Ti-Al-Ta ingots. As seen in this table, a significant burnout of Al up to 3.7 at.% occurred during plasma melting of the cold compacted materials. In addition, the content of O is significantly increased up to 1.31 at.% and the content of Ta exceeds the nominal composition by 0.6 at.%. The decrease of Al content can be explained by its evaporation due to a high temperature of the melt and highly inhomogeneous initial distribution of the pure metals within the semi-products. The increase of oxygen content up to 1.31 at.% can be attributed to: (i) insufficient rotary vacuum leading to a conservation of remaining air within the pores of the semi-products before flushing by argon and (ii) insufficient purity of the applied argon atmosphere (argon purity of 99.95 %). The increase of the Ta content up to 8.6 at.% can be attributed to the burnout of Al during melting, which was not compensated by adjusting chemical composition of the semi-products.

The chemical composition of the plasma melted Ti-Al-Ta ingots prepared from the binary Al-Ta master alloy, which was mixed with the Ti sponge, is close to the required nominal composition, as seen in Table 1. In this case, the content of Al in the master alloy is well adjusted to its expected burnout during melting. Since the content of Ta was kept at 8 at.% in the semi-products, its content in the plasma melted ingots exceeds by 0.9 at.% the nominal composition due to burnout of Al. The content of O is significantly reduced to 0.69 at.% when compared with the ingots prepared from the cold compacted semi-products. However, this content of oxygen is still sig-

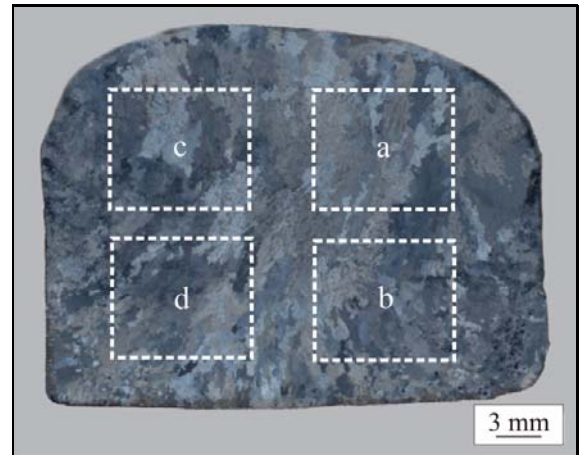


Fig. 8. OM showing the typical grain structure of plasma melted Ti-Al-Ta ingot prepared from the cold compacted semi-products. Positions of compression specimens is indicated by the rectangles a, b, c and d.

nificantly higher than a value of 0.26 at.% measured in the benchmark alloy, as seen in Table 1. Such high oxygen content in the plasma melted ingots can be explained by the contamination of the master Al-Ta alloy due to a reaction of the melt with the Al₂O₃-based crucible during induction melting.

3.3.2. Microstructure

Figure 8 shows the typical columnar and equiaxed grain structure on transverse sections of the plasma melted Ti-Al-Ta ingots. It should be noted that the grain structure is affected by multiple plasma passes and the height of the processed ingots.

Figure 9 shows the typical microstructure of the plasma melted ingots prepared from the cold compacted semi-products. Figure 9a illustrates the grain morphology in the region of columnar to equiaxed grain transition. An average diameter and length of the columnar grains is measured to be $(752 \pm 22) \mu\text{m}$ and $(3561 \pm 230) \mu\text{m}$, respectively. A mean diameter of the equiaxed grains is $(185 \pm 6) \mu\text{m}$. Cubic symmetry of the dendrites indicates that β phase (Ti-

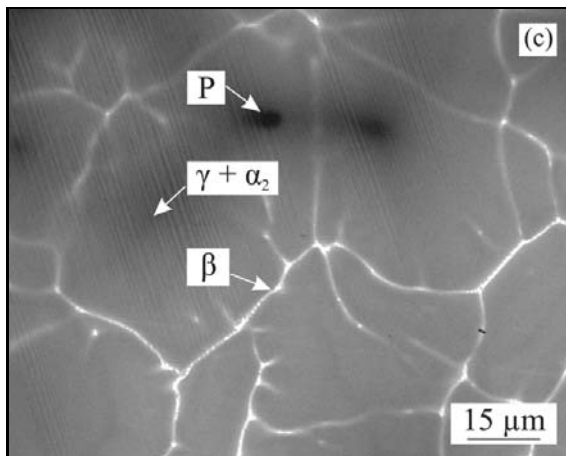
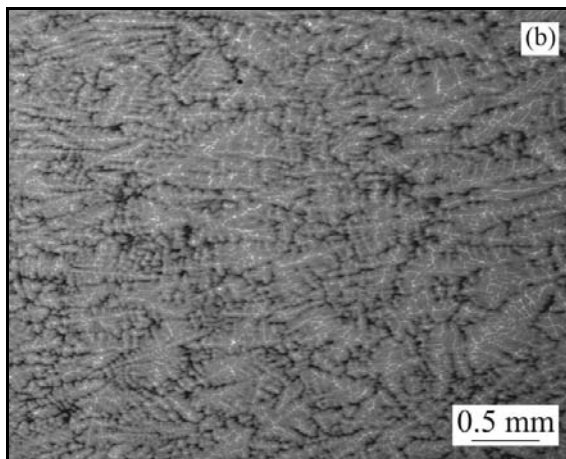
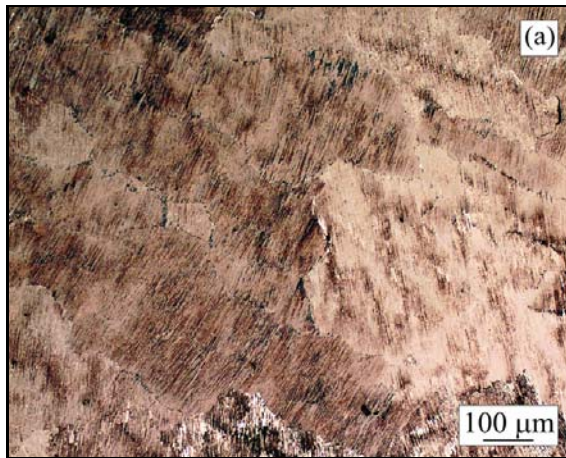


Fig. 9. Microstructure of plasma melted ingot prepared from the cold compacted semi-products: (a) OM micrograph showing the typical grain structure, (b) BSEM micrograph showing morphology and distribution of dendrites, (c) BSEM micrograph showing lamellar $\gamma + \alpha_2$ microstructure, network of remaining β phase and porosity P.

-based solid solution with cubic crystal structure) is the primary phase during solidification, as seen in Fig. 9b [21]. The microstructure of both colum-

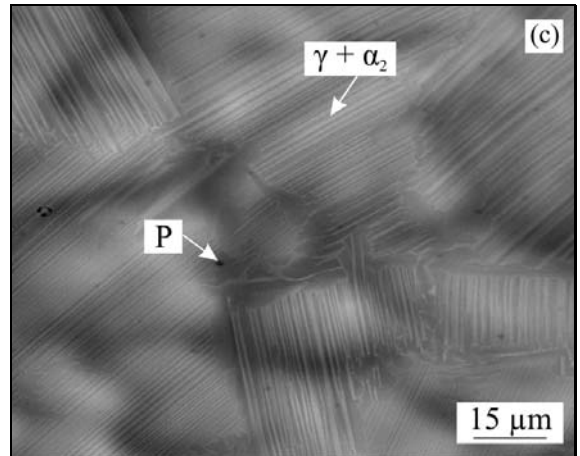
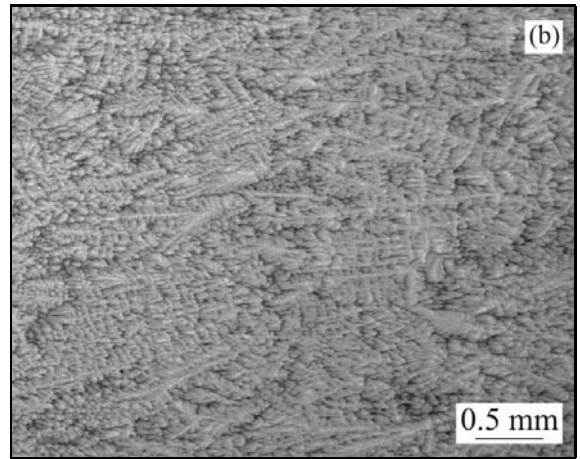
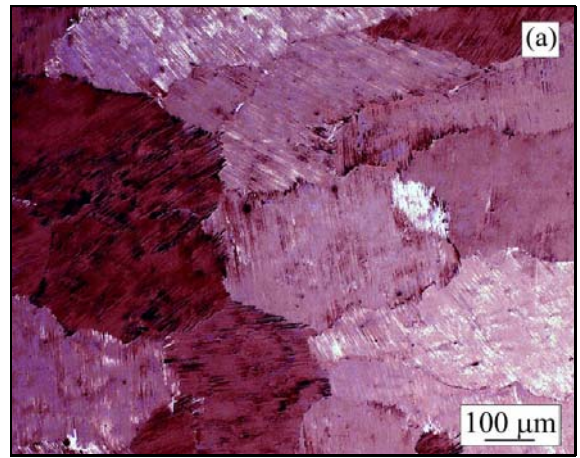


Fig. 10. Microstructure of plasma melted ingot prepared from the master Al-Ta alloy mixed with the Ti sponge: (a) OM micrograph showing the typical grain structure, (b) BSEM micrograph showing morphology and distribution of dendrites, (c) BSEM micrograph showing lamellar $\gamma + \alpha_2$ microstructure and porosity P.

nar and equiaxed grains is lamellar and consists of bright coloured $\alpha_2(\text{Ti}_3\text{Al})$ and dark coloured $\gamma(\text{TiAl})$ intermetallic phases [22], as shown in Fig. 9c.

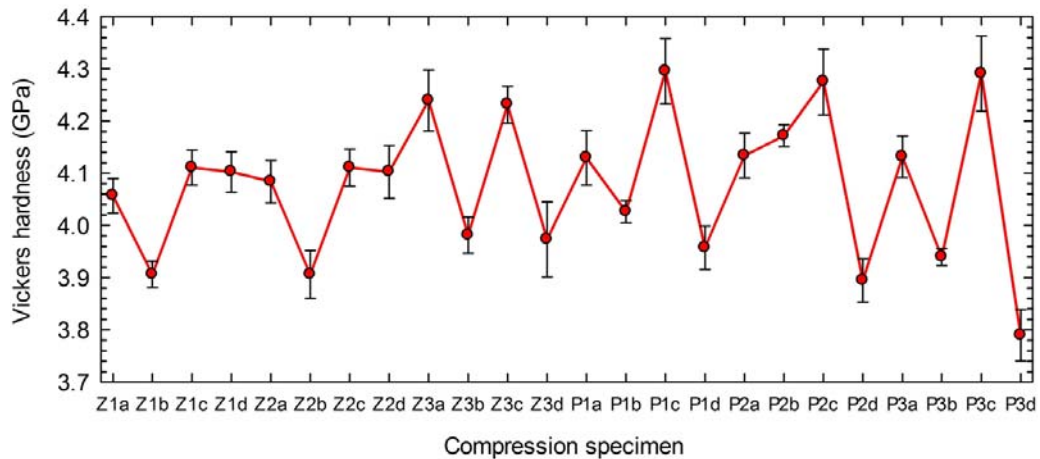


Fig. 11. Average Vickers hardness values of individual compression specimens: Z – specimens from the plasma melted ingot prepared from the cold compacted semi-products, P – specimens from the plasma melted ingot prepared from the master Al-Ta alloy mixed with the Ti sponge.

Mean interlamellar α_2 - α_2 spacing is measured to be (811 ± 16) nm. In addition, the microstructure contains a white coloured network, which is formed by the remaining β phase [21] and fine solidification porosity indicated in Fig. 9c.

Figure 10 shows the typical microstructure of the plasma melted ingots prepared from the master Al-Ta alloy, which was mixed with the Ti sponge. Figure 10a illustrates the grain morphology in the region of columnar to equiaxed grain transition. An average diameter and length of the columnar grains is measured to be (796 ± 27) μm and (4293 ± 253) μm , respectively. A mean diameter of the equiaxed grains is (220 ± 8) μm . Figure 10b shows cubic morphology of the dendrites which confirms the β primary solidification phase [21]. Figure 10c shows the typical lamellar $\gamma + \alpha_2$ microstructure with a mean interlamellar α_2 - α_2 spacing of (765 ± 14) nm and fine solidification porosity formed within columnar and equiaxed grains.

3.3.3. Mechanical properties

The specimens for Vickers hardness measurements and compression testing were prepared from the plates with a thickness of 7.5 mm, which were cut transversally in the positions 1, 2 and 3 (Fig. 7) from the plasma melted ingots. These plates were cut to smaller pieces with dimensions of $7.5 \times 7.5 \times 10$ mm³ and subjected to Vickers hardness measurements after grinding. Figure 11 shows average Vickers hardness of individual compression specimen designated as Zjk and Pjk , where Z is designated to the plasma melted ingot prepared from the cold compacted semi-products, P is designated to the plasma melted ingot prepared from the master Al-Ta alloy mixed with the Ti sponge, j is the position of compression specimen in the ingot (see Fig. 7 and marked positions 1, 2 and 3) and k represents the position of compression specimen on a trans-

verse section of the ingot (see Fig. 8 and marked positions a, b, c and d). The average Vickers hardness values vary between (3.89 ± 0.05) GPa and (4.29 ± 0.04) GPa. These values are significantly higher than that of (3.13 ± 0.01) GPa measured by Lapin et al. [23] for the benchmark heat treated Ti-46Al-8Ta (at.%) alloy with a convoluted $\gamma + \alpha_2$ type of microstructure. These differences in the Vickers hardness can be explained by a different chemical composition shown in Table 1 (variations in the content of Al, Ta and O) and fully lamellar microstructure of the plasma melted ingots when compared with those of the benchmark alloy. As shown by Lapin et al. [13, 24, 25], increase of oxygen content and decrease of interlamellar α_2 - α_2 spacing in TiAl-based alloys lead to an increase of Vickers hardness and microhardness.

Figure 12 shows 0.2 % offset compression yield strength (YS), compression strength (CS) and deformation to fracture measured on individual compression specimens at room temperature. An average YS is measured to be (817 ± 17) MPa and (776 ± 9) MPa for the plasma melted ingots prepared from the cold compacted semi-products (designated Z) and from the master Al-Ta alloy mixed with the Ti sponge (designated P), respectively. These values of the YS are higher than 0.2 % offset compression yield strength of 655 MPa measured by Lapin et al. [23] for the benchmark Ti-46Al-8Ta (at.%) alloy with the convoluted $\gamma + \alpha_2$ type of microstructure. In the case of the plasma melted ingot prepared from the cold compacted semi-products, this difference in the YS can be explained by a slightly different chemical composition of the ingot (lower Al content and slightly higher Ta content), fully lamellar microstructure and significantly higher oxygen content of 1.31 at.% when compared to that of 0.26 at.% measured in the benchmark alloy [23]. Oxygen is known to act as a solid solution strengthening element which increases yield strength

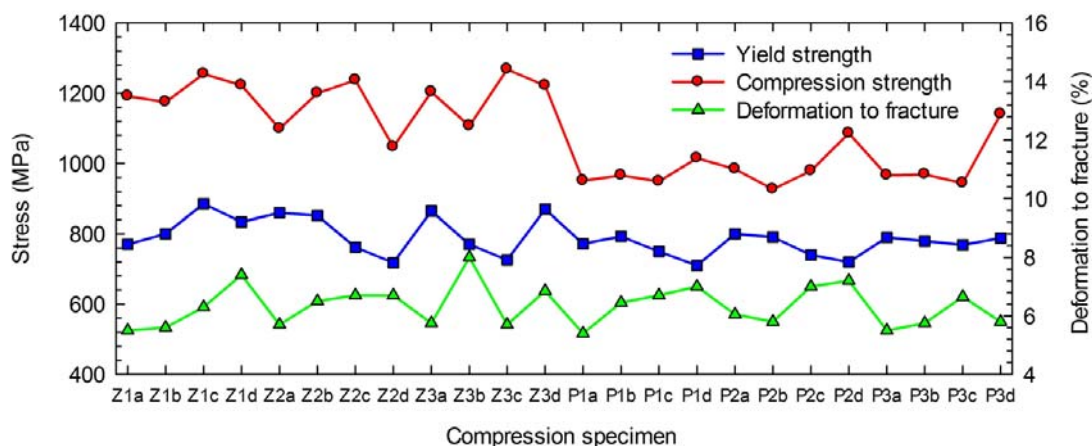


Fig. 12. Compression yield strength, compression strength and deformation to fracture of individual compression specimens: Z – specimens from the plasma melted ingot prepared from the cold compacted semi-products, P – specimens from the plasma melted ingot prepared from the master Al-Ta alloy mixed with the Ti sponge.

of TiAl-based alloys on the expense of decreasing room-temperature ductility [26]. An increase of the YS (776 MPa) of the plasma melted ingot prepared from the binary Al-Ta master alloy mixed with the Ti sponge when compared with that of the benchmark alloy (665 MPa) can be explained by higher content of Ta and O (Table 1) and fully lamellar microstructure (Fig. 10c). An average compression strength is measured to be (1186 ± 20) MPa and (990 ± 18) MPa for the plasma melted ingots prepared from the cold compacted semi-products and from the master Al-Ta alloy mixed with the Ti sponge, respectively. Generally, the CS of the plasma melted ingot prepared from the cold compacted semi-products is higher by 20 % than that of the ingot prepared from the binary Al-Ta master alloy mixed with the Ti sponge. This difference in the CS can be explained by different chemical composition (Table 1) and microstructure of the ingots (Figs. 9 and 10). For both types of the plasma melted ingots, an average compression deformation to fracture is measured to be (6.3 ± 0.6) % with some variations resulting mainly from some porosity within the compression specimens formed during solidification of the ingots in the cold hearth.

4. Conclusions

The investigation of the effect of two processing routes on chemical composition, microstructure and mechanical properties of plasma melted ingots with nominal composition Ti-46Al-8Ta (at.%) leads to the following conclusions:

1. Increase of compacting pressure from 215 to 645 MPa increases densification and force for disintegration of the cold compacted Ti-Al-Ta semi-products. An optimal compacting pressure is determined to be between 430 and 530 MPa. The applied pressures

lower than 430 MPa lead to an insufficient strength of the semi-products and the applied pressures higher than 530 MPa lead to a high wear of the metallic die.

2. During induction melting the stabilisation time of the melt ranging from 60 to 270 s has no significant effect on average chemical composition and homogeneity of the master Al-Ta alloy. Contamination of the master alloy by oxygen results from the reaction of the melt with Al_2O_3 -based crucible during melting.

3. The applied processing routes and selected optimal parameters of plasma melting result in a full dissolution of initial materials and homogeneous distribution of alloying elements in the plasma melted ingots prepared from the cold compacted Ti-Al-Ta semi-products as well as from the induction melted master Al-Ta alloy mixed with the Ti sponge.

4. The plasma melted ingots prepared from the cold compacted pure materials show high burnout of Al up to 3.7 at.% and contamination by O up to 1.31 at.%. Content of Al is well adjusted in the ingots prepared from the master Al-Ta alloy mixed with the Ti sponge and content of O is reduced to 0.69 at.%. However, both types of the plasma melted ingots have excess of Ta which was not adjusted by a change of nominal composition of the semi-products.

5. The plasma melted Ti-Al-Ta ingots contain columnar and equiaxed grains whose distribution depends on the height of the ingots. The morphology of dendrites indicates β (Ti-based solid solution) primary solidification phase in both types of ingots. The microstructure of the grains is lamellar and consists of $\alpha_2(\text{Ti}_3\text{Al})$ and $\gamma(\text{TiAl})$ intermetallic phases. The ingots prepared from the cold compacted semi-products contain remaining β phase in the form of a network.

6. Vickers hardness and compression yield strength of the plasma melted Ti-Al-Ta ingots are higher than those measured in the benchmark Ti-46Al-8Ta (at.%) alloy with convoluted $\gamma + \alpha_2$ type of microstructure.

The compression strength of the ingot prepared from the cold compacted semi-products is by 20 % higher than that of the ingot prepared from the master Al-Ta alloy mixed with the Ti sponge.

Acknowledgements

This work was financially supported by the Slovak Research and Development Agency under the contracts APVV-0434-10 and APVV-0009-07 and the Slovak Grant Agency for Science under the contract VEGA 2/0157/10. One author (J. Lapin) would like to acknowledge the support of the RMTVC project under the contract No. CZ.1.05/2.1.00/01.0040. The authors would like to thank to Ing. S. Demian, RNDr. T. Pelachová and Doc. Ing. L. Čaplovič, PhD. for help with plasma melting experiments, SEM and EDX measurements.

References

- [1] AGUILAR, J.—SCHIEVENBUSCH, A.—KÄTT-LITZ, O.: *Intermetallics*, 19, 2011, p. 757. [doi:10.1016/j.intermet.2010.11.014](https://doi.org/10.1016/j.intermet.2010.11.014)
- [2] TETSUI, T.—SHINDO, K.—KOBAYASHI, S.—TAKAYAMA, M.: *Scripta Mater.*, 47, 2002, p. 399. PII: S13 5 9-6 4 62 (02)00 1 5 8- 6
- [3] http://en.wikipedia.org/wiki/General_Electric_GENx
- [4] SHOUREN, W.—PEIQUAN, G.—LIYING, Y.: *J. Mater. Process. Tech.*, 204, 2008, p. 492. [doi:10.1016/j.jmatprotec.2008.01.062](https://doi.org/10.1016/j.jmatprotec.2008.01.062)
- [5] TETSUI, T.: *Mater. Sci. Eng. A*, 329–331, 2002, p. 582. PII: S0921-5093(01)01584-2
- [6] FU, P. X.—KANG, X. H.—MA, Y. C.—LIU, K.—LI, D. Z.—LI, Y. Y.: *Intermetallics*, 16, 2008, p. 130. [doi:10.1016/j.intermet.2007.08.007](https://doi.org/10.1016/j.intermet.2007.08.007)
- [7] GEBAUER, K.: *Intermetallics*, 14, 2006, p. 355. [doi:10.1016/j.intermet.2005.08.009](https://doi.org/10.1016/j.intermet.2005.08.009)
- [8] LAPIN, J.—GABALCOVÁ, Z.—PELACHOVÁ, T.: *Intermetallics*, 19, 2011, p. 396. [doi:10.1016/j.intermet.2010.11.007](https://doi.org/10.1016/j.intermet.2010.11.007)
- [9] LAPIN, J.—ONDRŮŠ, L.—NAZMY, M.: *Intermetallics*, 10, 2002, p. 1019. [doi:10.1016/S0966-9795\(02\)00119-X](https://doi.org/10.1016/S0966-9795(02)00119-X)
- [10] KUANG, J. P.—HARDING, R. A.—CAMPBELL, J.: *Mater. Sci. Technol.*, 16, 2000, p. 1007.
- [11] KUANG, J. P.—HARDING, R. A.—CAMPBELL, J.: *Int. J. Cast Metals Res.*, 13, 2001, p. 277.
- [12] APPEL, F.—WAGNER, R.: *Mater. Sci. Eng. R*, 22, 1998, p. 187. [doi:10.1016/S0927-796X\(97\)00018-1](https://doi.org/10.1016/S0927-796X(97)00018-1)
- [13] LAPIN, J.—GABALCOVÁ, Z.—BAJANA, O.: *Kovove Mater.*, 47, 2009, p. 159.
- [14] GÜTHER, V.—CHATTERJEE, A.—KETTNER, H.: In: *Gamma Titanium Aluminides 2003*. Eds.: Kim, Y.-W., Clemens, H., Rosenberger, A. H. USA, Warrendale, TMS 2003, p. 241.
- [15] WOOD, J. R.: In: *Gamma Titanium Aluminides 2003*. Eds.: Kim, Y.-W., Clemens, H., Rosenberger, A. H. USA, Warrendale, TMS 2003, p. 227.
- [16] HARDING, R. A.: *Kovove Mater.*, 42, 2004, p. 225.
- [17] SAAGE, H.—HUANG, A. J.—HU, D.—LORETTO, M. H.—WU, X.: *Intermetallics*, 17, 2009, p. 32. [doi:10.1016/j.intermet.2008.09.006](https://doi.org/10.1016/j.intermet.2008.09.006)
- [18] HU, D.—HUANG, A. J.—WU, X.: *Intermetallics*, 15, 2007, p. 327. [doi:10.1016/j.intermet.2006.07.007](https://doi.org/10.1016/j.intermet.2006.07.007)
- [19] LAPIN, J.—PELACHOVÁ, T.—WITUSIEWICZ, V. T.—DOBROČKA, E.: *Intermetallics*, 19, 2011, p. 121. [doi:10.1016/j.intermet.2010.09.016](https://doi.org/10.1016/j.intermet.2010.09.016)
- [20] WITUSIEWICZ, V. T.—BONDAR, A. A.—HECHT, U.—ZOLLINGER, J.—PETYUKH, V. M.—FOMICHOV, O. S.—VOBLIKOV, V. M.—REX, S.: *Intermetallics*, 18, 2010, p. 92. [doi:10.1016/j.intermet.2009.06.015](https://doi.org/10.1016/j.intermet.2009.06.015)
- [21] LAPIN, J.—GABALCOVÁ, Z.: *Intermetallics*, 19, 2011, p. 797. [doi:10.1016/j.intermet.2010.11.021](https://doi.org/10.1016/j.intermet.2010.11.021)
- [22] LAPIN, J.—PELACHOVÁ, T.—DOMÁNKOVÁ, M.: *Intermetallics*, 19, 2011, p. 814. [doi:10.1016/j.intermet.2010.11.023](https://doi.org/10.1016/j.intermet.2010.11.023)
- [23] LAPIN, J.—GABALCOVÁ, Z.—PELACHOVÁ, T.—BAJANA, O.: *Materials Science Forum*, 638–642, 2010, p. 1368. [doi: 10.4028/www.scientific.net/MSF.638-642.1368](https://doi.org/10.4028/www.scientific.net/MSF.638-642.1368)
- [24] LAPIN, J.—GABALCOVÁ, Z.: *Kovove Mater.*, 46, 2008, p. 185.
- [25] LAPIN, J.: *J. Mater. Sci. Lett.*, 22, 2003, p. 747. [doi: 10.1023/A:1023708110793](https://doi.org/10.1023/A:1023708110793)
- [26] LAMIRAND, M.—BONNENTIEN, J.-L.—FERRIÈRE, G.—GUÉRIN, S.—CHEVALIER, J.-P.: *Scripta Mater.*, 56, 2007, p. 325. [doi:10.1016/j.scriptamat.2006.11.024](https://doi.org/10.1016/j.scriptamat.2006.11.024)